Research article

Ming Zhang, Fei Zhang, Yi Ou, Jixiang Cai and Honglin Yu*

Broadband terahertz absorber based on dispersion-engineered catenary coupling in dual metasurface

https://doi.org/10.1515/nanoph-2018-0110
Received August 2, 2018; revised September 11, 2018; accepted October 2, 2018

Abstract: Terahertz (THz) absorbers have attracted considerable attention due to their potential applications in high-resolution imaging systems, sensing, and imaging. However, the limited bandwidth of THz absorbers limits their further applications. Recently, the dispersion management of metasurfaces has become a simple strategy for the bandwidth extension of THz devices. In this paper, we used the capability of dispersion management to extend the bandwidth of THz absorbers. As a proof-of-concept, a dual metasurface-based reflective device was proposed for broadband near-unity THz absorber, which was composed of two polarization-independent metasurfaces separated from a metallic ground by dielectric layers with different thickness. Benefiting from the fully released dispersion management ability in adjusting the dimensions of the metasurfaces, we obtained an absorbance above 90% in the frequency range from 0.52 to 4.4 THz and the total thickness for the bandwidth approaching the theoretical Rozanov limit. The experimental results verified the ability of dispersion management in designing broadband absorbers and the performance of the designed absorber. The underlying physical mechanism of dispersion management was interpreted in the general equivalent circuit theory and transmission line model. In addition, the catenary optical model was used to further interpret the physics behind this dual metasurface. Moreover, we found that the alignment deviations between the dual metasurface had little impact on the performance of the designed absorber, which indicates that the dual-metasurface does not require center alignment and is easy to be fabricated. The results of this work could broaden the application areas of THz absorbers.

Keywords: metasurfaces; terahertz absorbers; dispersion management; catenary optics.

***Corresponding author: Honglin Yu,** Key Laboratory of Opto-electronic Technology and Systems of the Education Ministry of China, Chongqing University, Chongqing 400044, China, e-mail: hlyu@cqu.edu.cn
Ming Zhang, Fei Zhang, Yi Ou and Jixiang Cai: Key Laboratory of Opto-electronic Technology and Systems of the Education Ministry of China, Chongqing University, Chongqing 400044, China

1 Introduction

In recent years, terahertz (THz) electromagnetic waves with the frequency range from 0.1 to 10 THz have become the hotspot of research. Benefiting from the newly emerging metamaterials, THz devices have spawned a series of significant applications in many kinds of fields such as imaging spectrum systems communications, and non-destructive sensing [1–5]. Among these applications, THz absorbers have become the crucial component. Since Landy et al. first proposed the concept of metamaterial absorbers (MMAs) [6], MMAs have attracted great research attention. The mechanism of MMAs to realize the near-perfect absorption is the impedance matching with the surrounding air. Recently, different kinds of MMA designs with matched impedance have been investigated in a wide frequency region [7–12]. However, these perfect MMAs usually work in a narrow band, typically not more than 20% of the center frequency, which is caused by their resonance features. Nevertheless, broadband absorption is highly desirable in many applications, such as electromagnetic stealth, detectors, and THz imaging [8, 13, 14].

Thus far, a lot of efforts have been made to break the bandwidth limitation of THz absorbers. Typically, the common approaches to extend operation bandwidth are stacking multiple layers consisting of different antenna arrays and constructing composite supercell with different resonance modes. In 2014, Zhu et al. implemented a metal-dielectric multilayer composite to realize a broadband absorber with an absorption above 80% and a full-width at half-maximum of 127% in the range of 0.7–2.3 THz [15]. In 2017, Kenney et al. proposed a planar THz absorber

composed of a supercell of fractal crosses to acquire an average absorption of 83% from 2.82 to 5.15 THz [16]. These works demonstrated the ability to broaden the bandwidth of the approaches but at the expense of a complex supercell or an increased fabrication complexity. A strategy to fix the problems is engineering heavily doped silicon. In 2012, Pu et al. initially exploited the heavily doped silicon to realize broadband absorption. Then, they proposed a binary grating structure on heavily doped silicon to acquire an absorption larger than 90% in frequencies from 1 to 4 THz [17]. Then, a lot of works based on doped silicon realized broadband absorption in the THz region [18–21]. These works have made a great progress in broadband THz absorbers. However, fabrication is complex in multilayer doped silicon and the bandwidth needs to be further improved. Recently, a better strategy, dispersion management of metasurfaces for bandwidth extension, has been proposed [22–24]. By conjugating the compensation of the dispersion of metasurfaces and the frequency-dependent phase shift of the dielectric spacing layer, ultra-broadband THz devices can be realized. In particular, with the help of coherent control, ultra-broadband absorption with ultrathin film has been demonstrated [25], which breaks the fundamental limitation of bandwidth and thickness.

In this paper, we used the capability of dispersion management to extend the bandwidth of THz absorbers. As a proof-of-concept, a metamirror with the dual-metasurface was designed for a broadband near-unity THz absorber, which was composed of two polarization-independent metasurfaces separated from a metallic ground by dielectric layers with different thickness. Benefiting from the fully released dispersion management ability in adjusting the dimensions of the metasurface, we obtained the ultra-broadband THz absorber in the frequency range from 0.52 to 4.4 THz with an absorbance above 90%. The experimental results verified the ability of dispersion management in designing broadband absorbers and the performance of the designed absorber. The underlying physical mechanism of dispersion management was interpreted in the general equivalent circuit theory and transmission line model. Besides, we employed catenary electric fields to further interpret the physics behind the dual-metasurface. The absorber is polarization insensitive due to the symmetry of dual metasurfaces. Importantly, we investigated the impact of alignment deviation between the dual metasurfaces on the performance of designed absorber and simulated results showed a slight declination, which make it easy to be fabricated. We believe that the ultra-broadband absorber could find important applications in THz devices.

2 Structure and results

The schematic of the array and unit cell of this ultra-broadband THz absorber is shown in Figure 1A and B. The absorber consists of dual metasurfaces separated from the metallic ground plane by SU-8 photoresist layers with different thickness (i.e. metamirror), and an extra SU-8 layer is capped on top of the metasurface. Figure 1C and D gives the top views of the dual metasurfaces. The metasurfaces are composed of arrays of square loops and patches, and metasurface 2 has twice the period of metasurface 1. The metallic parts are both made up of chromium with a conductivity of 2.2×10^5 S/m, and the thickness of the ground plane and dual metasurface are 300 and 150 nm, respectively. The permittivity of SU-8 photoresist is $2.79+i0.31$ [15], and the thicknesses of trilayer insulators are $h_1=20$ μm, $h_2=16$ μm, and $h_3=20$ μm. The other detailed geometric parameters of the broadband THz absorber are optimized as $P=2\times P_1=100$ μm, $l_1=35$ μm, $l_2=23$ μm, $l_3=80$ μm, $l_4=60$ μm, and $w=16$ μm.

The broadband THz absorber was investigated with a commercial software package (CST Microwave Studio) using the finite-element method. In the simulations, the unit cell boundary conditions were applied in the x and y directions, whereas the top and bottom boundaries normal to the z-axis were set as open. Due to the symmetry of the structure, we applied the normally incident TM-polarized plane wave with the polarization of the electric field along the x direction. The absorption of the THz absorber $A(\omega)$ can be calculated by

$$A(\omega)=1-T(\omega)-R(\omega) \tag{1}$$

where $T(\omega)$ and $R(\omega)$ are the transmittance and reflectance of the absorber, respectively. Because the metallic ground plane is thick enough to prevent the THz wave transmission, the absorption can be simplified as $A(\omega)=1-R(\omega)$. Figure 1E shows the calculated absorption spectra of the ultra-broadband THz absorber in the frequency range from 0 to 5 THz. As depicted in Figure 1E, the incident THz wave ranging from 0.52 to 4.4 THz can be efficiently absorbed with an absorption above 90%, and the corresponding relative absorption bandwidth is nearly 143%. For a physically realizable broadband absorber, the Rozanov limit indicates that, for any metal-backed absorber under a normal incidence, its total thickness d must be larger than a theoretical limit for the given frequency response of the absorption [21], i.e.

$$\left|\int_0^\infty \ln\left|R(\lambda)\right| d\lambda\right| \le 2\pi^2 d \tag{2}$$

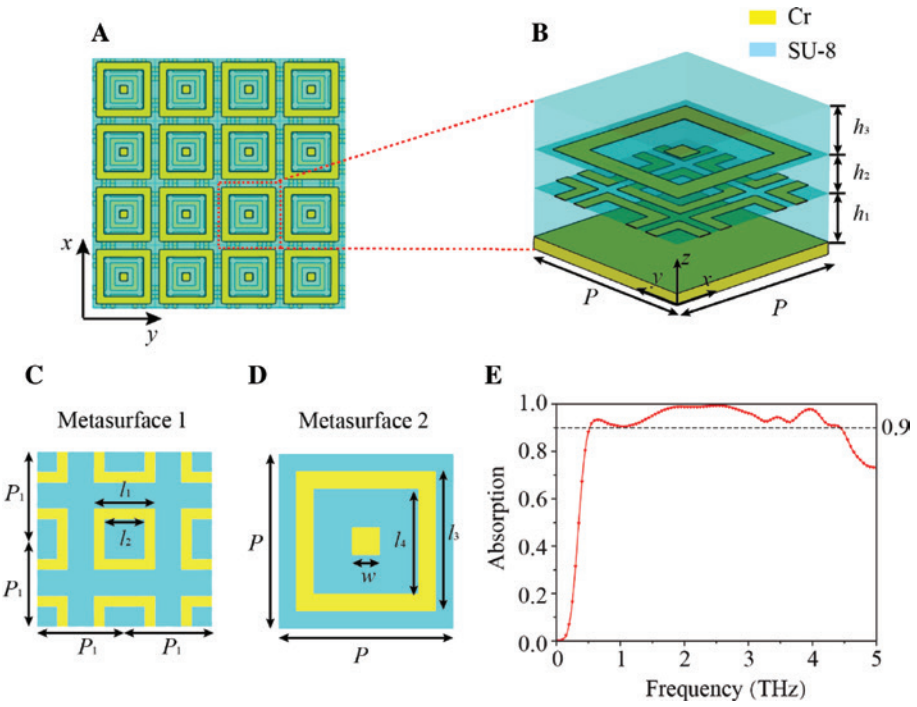

Figure 1: Schematic structure of the broadband THz absorber and simulated results.
(A) Top view of the arrays. (B) Three-dimensional schematic diagram. Top views of (C) metasurface 1 and (D) metasurface 2 with geometric parameters. (E) Simulated absorption spectra at normal incidence in the frequency range from 0 to 5 THz.

where λ is the free-space wavelength. For the broadband absorption shown in Figure 1E, the corresponding theoretical limit is estimated to be 53.07 μm, which is close to the thickness (56 μm) of the designed absorber.

To prove the simulated results, a sample was fabricated by a standard optical lithography process by employing the same structural and material parameters used in the above simulations (more fabrication details are depicted in the supplementary material). Figure 2A and B shows the optical microscopy image of the fabricated sample. The sample was measured by a commercial THz-time domain spectroscopy (THz-TDS; ADVANTEST TAS7400SP) with a frequency range from 0.1 to 1.5 THz. In the measurement, an opaque gold film was used as the reference reflection mirror. Figure 2C depicts the measured results at an incident angle of 20°, which is the minimum incident angle of THz-TDS for TE and TM polarizations. For a broader study of the THz properties, the sample was also characterized by a Fourier transform infrared (FTIR; Bruker v80) spectroscope equipped with a bolometer detector that offered a valid range from 1.5 to 5 THz. The measured spectral characterization was obtained using an 11° angle reflection accessory. Figure 2D gives the measured result under polarization-independent incidence due to the lack of a linear-polarized plate in this frequency range. From the spectrum, we can obtain an absorbance that exceeds the 90% range from 1.8 to 4 THz. Looking at the measured absorption rate in Figure 2 as a whole, the fabricated THz absorber remains a high absorbance (almost more than 90%) in the designed frequency range. The measured results agree well with the simulated results in all, which demonstrates the ultra-broadband and high absorbance of the absorber. Note that there is also deviation between measured results and simulated results, which may be caused by the fabricated imperfection and accuracy of measured instrument. Besides, an oblique incident angle makes a slight difference of absorption between TE and TM polarizations (as depicted in Figure 2C).

3 Theoretical analysis

Subsequently, we resort to the transmission line model and general equivalent circuit theory to interpret the underlying physical mechanism of the broadband absorber. Due to the deep-subwavelength thickness, such dual-metasurface layer can be regarded as thin impedance sheets. We present an analytical circuit model to interpret the sheet impedance. In this case, arm and gap behave as inductors

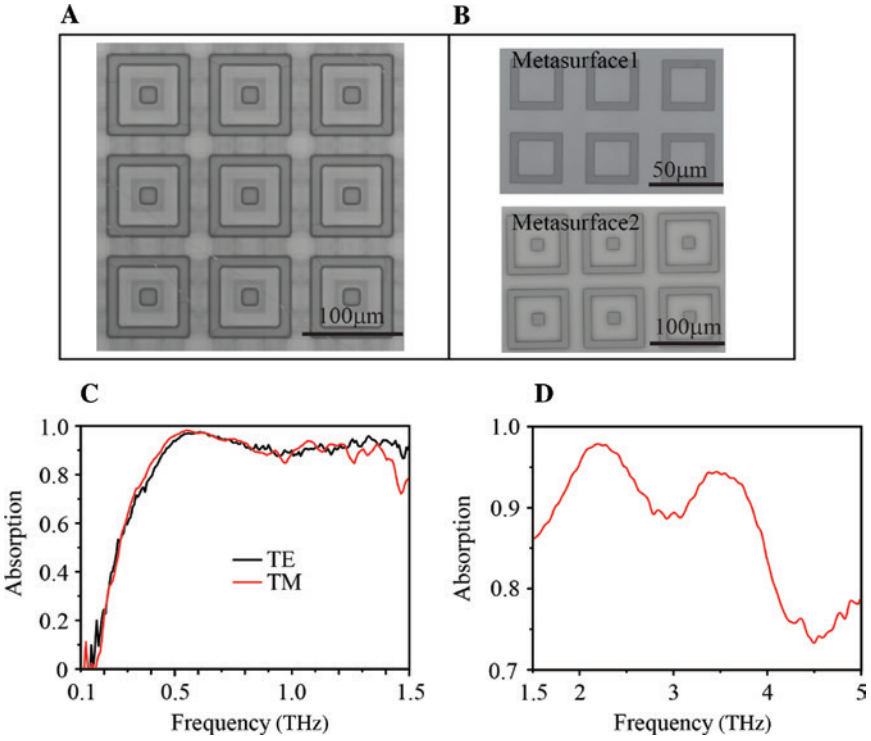

Figure 2: Optical microscopy image and measured absorption of the THz absorber.
Optical microscopy images of the whole structure (A) and dual metasurface (B). Absorption measured by THz-TDS in the frequency range from 0.1 to 1.5 THz (C) and measured by FTIR in the frequency range from 1.5 to 5 THz (D).

and capacitors, respectively. Figure 3A and B shows the general equivalent circuit theory for the dual metasurface, and according to the classic circuit, the frequency-dependent impedance can be expressed as [26, 27]

$$Z_{s1} = R_1 + j\omega L_1 + \frac{1}{j\omega C_1} \tag{3}$$

$$Z_{s2} = R_s + \frac{Z_{g1}Z_{g2}}{Z_{g1} + Z_{g2}} \tag{4}$$

First, we consider the equivalent impedance of metasurface 2. In Equation (4), Z_{g1} and Z_{g2} are the equivalent frequency-dependent impedance of two resonant circuits in metasurface 2. Besides, Z_{g1} and Z_{g2} can be expressed as

$$Z_{g1} = j\omega L_{s1} + \frac{1}{j\omega C_{s1}} \tag{5}$$

$$Z_{g2} = \frac{1}{j\omega C_{s2}} \tag{6}$$

The equations for calculating the resistance, capacitance, and inductance in the equivalent circuit can be expressed as [28, 29]

$$R_s = R_0 \frac{p_2^2}{2d_2 w_2 + d_3^2} \tag{7}$$

$$L_{s1} = \frac{F(p_1, 2w_2, \lambda)}{\omega} \tag{8}$$

$$C_{s1} = \frac{0.75 \times 4 d_2 \varepsilon_{\text{eff}}}{\omega p_2} F(p_2, g_{s1}, \lambda);\ C_{s2} = \frac{d_3}{\omega p_1}\left(\frac{C'C''}{C' + C''}\right) \tag{9}$$

$R_0 = 1/(\sigma_{\text{Cr}} t)$ is the resistance of Cr film (σ_{Cr} and t are the conductivity and thickness of chromium, respectively). ε_{eff} is the permittivity of SU-8 photoresist. In Equation (9), C' and C'' are induced by the outer and inner gaps, which can be expressed as

$$C' = \frac{4\varepsilon_{\text{eff}} F(p_2, g_{s1}, \lambda)}{\omega} \tag{10}$$

$$C'' = \frac{4\varepsilon_{\text{eff}} F(p_2, g_{s2}, \lambda)}{\omega} \tag{11}$$

In addition, F can be expressed as

$$F(p, s, \lambda) = \frac{p}{\lambda}\cos\theta\left(\ln\left[\csc\left(\frac{\pi s}{2p}\right)\right] + G(p, s, \lambda)\right) \tag{12}$$

θ is the angle of incidence, λ is the wavelength, and G is the correction term [29]. Interestingly, the first term of Equation (12) is characterized by the catenary of equal strength, which was called catenary dispersion [30]. In the same way, we can obtain the resistance, inductance, and capacitance in the general equivalent circuit theory of metasurface 1 as follows:

$$R_1 = R_0 \frac{p_1^2}{2d_1 w_1} \tag{13}$$

$$L_1 = \frac{d_1}{\omega p_1} F(p_1, 2w_1, \lambda) \tag{14}$$

$$C_1 = \frac{4d_1 \varepsilon_{\text{eff}}}{\omega p_1} F(p_1, g_1, \lambda) \tag{15}$$

Assuming that a plane wave normally impinges on the metamirror, due to reflections occurring at the metasurface and background plane, both the forward and backward scattering waves exist in the dielectric spacer and surrounding space, as depicted in Figure 3C. According to the transmission line model, we can obtain the general equivalent circuit theory of the THz absorber, as shown in Figure 3D. Z_{s1} and Z_{s2} are the equivalent impedance of the dual metasurfaces. Z_{d1}, Z_{d2}, and Z_{d3} are the characteristic impedance of trilayer SU-8 colloids, respectively. β_0 and β_d are the propagation constant of the free space and medium, respectively. Z_0 and Z_{in} are the characteristic impedance of free space and input impedance of the whole circuit model. The input impedance of each layer can be described as [31]

$$Z_{L\_i} = \frac{Z_{si} Z_{in\_i}}{Z_{si} + Z_{in\_i}} \tag{16}$$

$$Z_{in\_(i+1)} = Z_{di} \frac{Z_{L\_i} + jZ_{d(i+1)} \tan(\beta_d d_{(i+1)})}{Z_{d(i+1)} + jZ_{L\_i} \tan(\beta_d d_{(i+1)})} \tag{17}$$

In Equations (14) and (15), β_d and Z_{di} (i=1, 2) can be expressed as

$$\beta_d = \frac{\omega \sqrt{\varepsilon_d (1 - j \tan\delta)}}{c} \tag{18}$$

$$Z_d = \eta_0 \frac{1}{\sqrt{\varepsilon_d (1 - j \tan\delta)}} \tag{19}$$

$\eta_0 \approx 377\Omega$ is the free-space impedance. ε_d and $\tan\delta$ are the relative permittivity and dielectric dissipation factor of SU-8 colloids, respectively. Using the iterative algorithm, we can recursively derive the input impedance of the

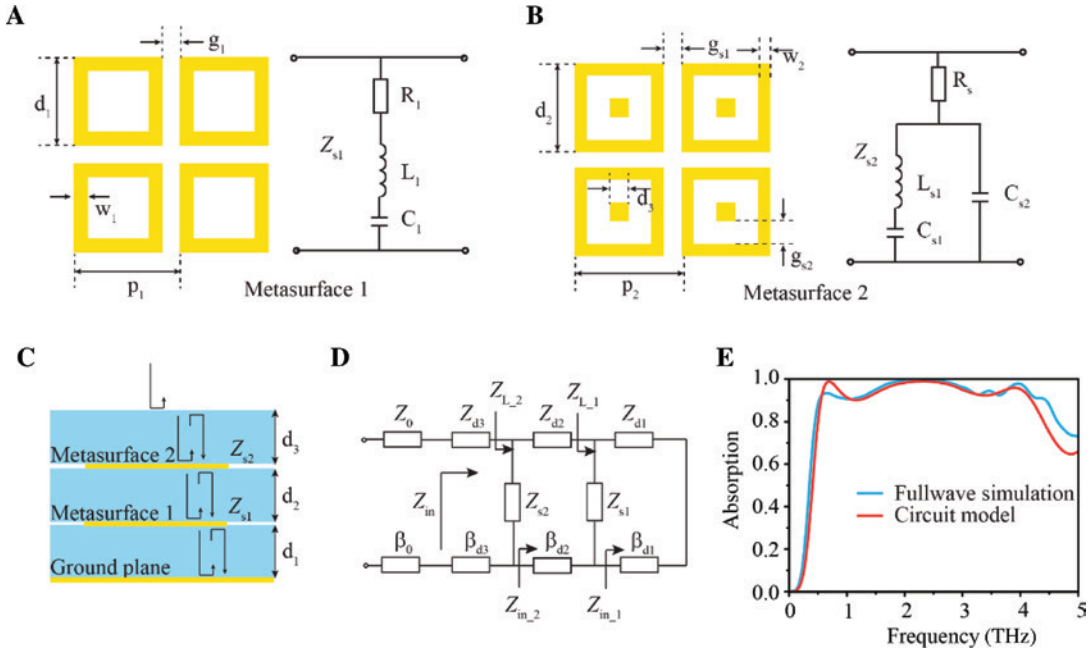

Figure 3: Theoretical simulations of the broadband THz absorber.
Geometric parameters and the corresponding general equivalent circuit theory for metasurface 1 (A) and metasurface 2 (B). (C) Schematic of the transmission line model for broadband THz absorption. (D) Equivalent circuit model of the structure with the dual metasurface based on the metamirror. (E) Comparison of the calculated absorption obtained with full-wave simulation and the circuit model.

entire general equivalent circuit theory from the bottom layer. The reflection coefficient can be calculated by the following equation:

$$\Gamma = \frac{Z_{in} - Z_0}{Z_{in} + Z_0} \tag{20}$$

Then, we can calculate the absorbance of the proposed broadband absorber by the simplified form of Equation (1). The theoretical results of the transmission line model are shown in Figure 3E, which shows good agreement with the numerical results by full-wave simulation. Based on this approach, we can further expand the bandwidth of the THz absorber by stacking more metasurfaces.

In an effort to further illustrate the relationship between the effective impedance and the geometry of the metasurface, the amplitude of electric field for the dual metasurfaces in the *x-z* plane at resonant frequencies (0.6 and 2.5 THz) is plotted in Figure 4A, C, D, and F. In addition, we illustrate the instantaneous electric field distributions under normal incidence at these resonant frequencies, which is depicted in Figure 4B and E. Apparently, the strong resonance occurred in the gap of the adjacent unit cell are responsible for the absorption at low frequency (0.6 THz). For higher frequency (2.5 THz), the resonance occurred in the gap of a single unit cell; additionally, there appears a hybrid mode between the two metasurfaces. To take a closer look at this issue, we employed the extracted E-field amplitude at these resonances. Interestingly, all profiles in the gaps can be well described by the well-known catenary curves in architecture (the fitting curves are shown in blue solid lines and the generalized catenary model is given in the supplementary material). Due to the THz frequency range, metal can be treated as the perfect electric conductor (as mentioned above) and surface plasmon polaritons do not exist. Thus, the amplitude of the E-field along the center of the gap can be fitted with a curve using the catenary function, and excellent agreement is found [32, 33]. This catenary optical field is also called as microscopic meta-surface-wave (M-wave) [34]. When changing the geometry of the metasurface, the catenary field distributions will be altered as well, leading to the modulation of the effective impedance at the corresponding metasurface. By properly optimizing the profile of the catenary field and coupling the different catenary field in structure, the desired effective impedance

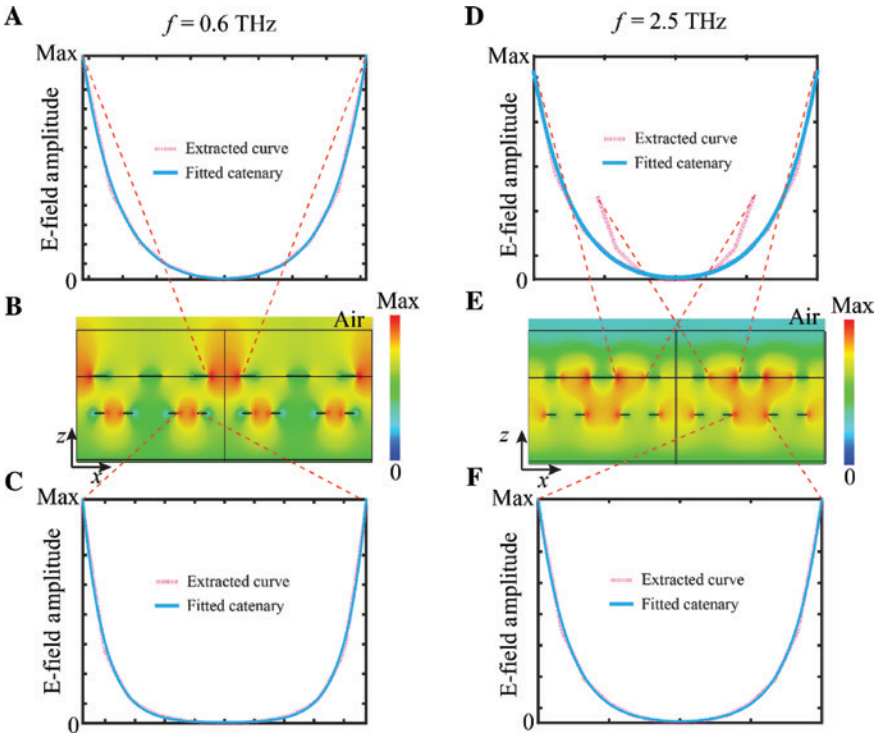

Figure 4: The analytical catenary field model of dual-metasurface.
Extracted electric field amplitude (red dotted line) and fitting catenary curve (blue solid line) between two arms of the resonator and adjacent resonators for the dual metasurface at 0.6 THz (A and C) and 2.5 THz (D and F), respectively. The slightly discrepancy is because the extracted field is the superposition of the catenary field (evanescent field) and incident field. (B and E) Electric field distribution in the *x-z* plane at two resonant frequencies.

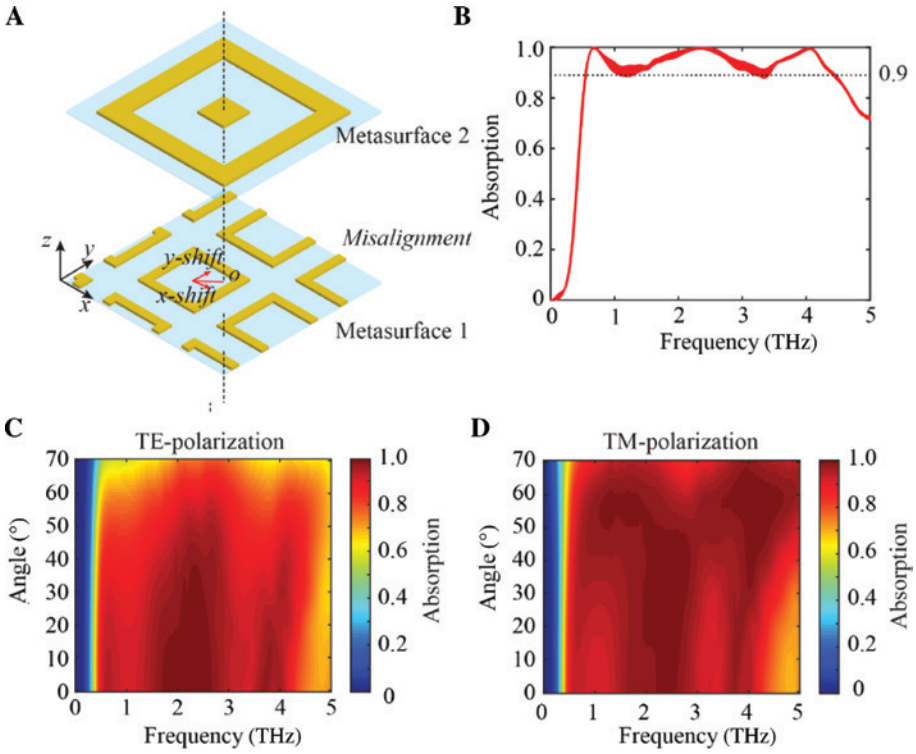

Figure 5: (A) Schematic image of the misalignment between the dual metasurface. (B) Simulated absorption performance when the dual metasurface is misaligned. Simulated absorption of the designed absorber as functions of the incident angle and working frequency for TE (C) and TM (D) polarizations.
The normalized absorption is represented by different colors.

of metasurfaces can be obtained, thus achieving broadband absorption. The discrepancy between the extracted field and the fitted catenary in Figure 4D is caused by the coupling of closely adjacent catenary field in metasurface 1, which implies a hybrid mode. Akin to the dispersion management (general equivalent circuit theory and transmission line model), we believe that this catenary E-field model offers a new interpretation to understand the physics behind resonance-based metasurfaces. Based on the above analysis, engineering the dispersion of metasurfaces has the potential to realize broadband absorption.

Then, we investigated the impact of the alignment deviation between the dual metasurfaces on the performance of the THz absorber. The parameters *x*- and *y*-shifts (as depicted in Figure 5A) represent the deviation distance between the dual metasurfaces along the *x* and *y* directions. The range of *x*- and *y*-shifts is from –25 to 25 μm, including the strict alignment to the maximum deviation. The simulated results of the parameter sweep of *x*- and *y*-shifts with an increment of 1 μm are plotted as a band in Figure 5B. The results reveal that the performance of the broadband high-efficiency THz absorber is sustained in all cases. Thus, the designed absorber exhibits high manufacturing tolerance, which makes the absorber easy to be fabricated. For practical applications, the incident THz wave is not always impinging normally into the THz devices. Therefore, we have to investigate the performance of the absorber under oblique incidence. The simulated absorption at different incidence angles for TE and TM polarizations are shown in Figure 5C and D. For TE polarization (Figure 5C), the absorption intensity drops when the incident angles are larger than 50°, but the bandwidth seems to experience little changes. For TM polarization (Figure 5D), the absorption intensity has weak dependence on the incident angle even up to 70°. The results indicate that the absorber remains at high performance in the case of wide-angle incidence.

4 Conclusion

In summary, we apply the dispersion management for metamirror with the dual-metasurface to extend the operating bandwidth of the THz absorber. As a proof-of-concept, an ultra-broadband THz absorber with an operating bandwidth range from 0.52 to 4.4 THz is designed and experimentally characterized. As the general equivalent circuit theory and transmission line model confirm that

the broadband absorption is induced by the coupling of multiple resonances in dual metasurface, broader bandwidth and better performance could be obtained by stacking more metasurfaces or adopting elaborate metasurface. With the help of the catenary optical model, we can better understand the E-field distribution of the metasurface at resonant frequency and design the structures more efficiently. Moreover, ignoring the deviation of the alignment makes the absorber closer to the applications and potential for further bandwidth extension. The strategy of dispersion management to extend the working bandwidth can be also applied for other designs of broadband metamaterial-based devices.

See the supplementary material for the supporting content.

Acknowledgments: The authors declare no competing financial interest. We thank Ms. Yuan for her help with the fabrication. This work was supported by the National Natural Science Funds of China (grant 61575032).

References

[1] Darmo J, Tamosiunas V, Fasching G, et al. Imaging with a terahertz quantum cascade laser. Opt Express 2004;12:1879.
[2] Federici JF, Schulkin B, Huang F, et al. THz imaging and sensing for security applications – explosives, weapons and drugs. Semicond Sci Technol 2005;20:S266–80.
[3] Ferguson B, Zhang XC. Materials for terahertz science and technology. Nat Mater 2002;1:26–33.
[4] Liu X, Starr T, Starr AF, et al. Infrared spatial and frequency selective metamaterial with near-unity absorbance. Phys Rev Lett 2010;104:207403.
[5] Luo X. Subwavelength optical engineering with metasurface waves. Adv Opt Mater 2018;6:1701201.
[6] Landy NI, Sajuyigbe S, Mock JJ, et al. Perfect metamaterial absorber. Phys Rev Lett 2008;100:207402.
[7] Zhang M, Fang J, Zhang F, et al. Ultra-narrow band perfect absorbers based on Fano resonance in MIM metamaterials. Opt Commun 2017;405:216–21.
[8] Grant J, Ma Y, Saha S, et al. Polarization insensitive, broadband terahertz metamaterial absorber. Opt Lett 2011;36:3476–8.
[9] Taylor AJ, Chowdhury DR, Chen HT, et al. Experimental demonstration of terahertz metamaterial absorbers with a broad and flat high absorption band. Opt Lett 2012;37:154–6.
[10] Kim DS, Kim DH, Hwang S, et al. Broadband terahertz absorber realized by self-assembled multilayer glass spheres. Opt Express 2012;20:13566–72.
[11] Huang Y, Liu L, Pu M, et al. A refractory metamaterial absorber for ultra-broadband, omnidirectional and polarization-independent absorption in the UV-NIR spectrum. Nanoscale 2018;10:8298–303.
[12] Huang Y, Pu M, Gao P, et al. Ultra-broadband large-scale infrared perfect absorber with optical transparency. Appl Phys Express 2017;10:112601.
[13] Iwaszczuk K, Strikwerda AC, Fan K, et al. Flexible metamaterial absorbers for stealth applications at terahertz frequencies. Opt Express 2012;20:635–43.
[14] Landy NI, Bingham CM, Tyler T, et al. Design, theory, and measurement of a polarization insensitive absorber for terahertz imaging. Phys Rev B 2009;79:125104.
[15] Zhu J, Ma Z, Sun W, et al. Ultra-broadband terahertz metamaterial absorber. Appl Phys Lett 2014;105:4773–9.
[16] Kenney M, Grant J, Shah YD, et al. Octave-spanning broadband absorption of terahertz light using metasurface fractal-cross absorbers. ACS Photonics 2017;4:2604–12.
[17] Pu M, Wang M, Hu C, et al. Engineering heavily doped silicon for broadband absorber in the terahertz regime. Opt Express 2012;20:25513–9.
[18] Yin S, Zhu J, Xu W, et al. High-performance terahertz wave absorbers made of silicon-based metamaterials. Appl Phys Lett 2015;107:073903.
[19] Peng Y, Zang X, Zhu Y, et al. Ultra-broadband terahertz perfect absorber by exciting multi-order diffractions in a double-layered grating structure. Opt Express 2015;23:2032–9.
[20] Shi C, Zang XF, Wang YQ, et al. A polarization-independent broadband terahertz absorber. Appl Phys Lett 2014;105:033101–348.
[21] Rozanov NK. Ultimate thickness to bandwidth ratio of radar absorbers. IEEE Trans Antennas Propag 2000;48:1230–4.
[22] Pu M, Zhao Z, Wang Y, et al. Spatially and spectrally engineered spin-orbit interaction for achromatic virtual shaping. Sci Rep 2015;5:9822.
[23] Guo Y, Yan L, Pan W, et al. Achromatic polarization manipulation by dispersion management of anisotropic meta-mirror with dual-metasurface. Opt Express 2015;23:27566.
[24] Feng Q, Pu M, Hu C, et al. Engineering the dispersion of metamaterial surface for broadband infrared absorption. Opt Lett 2012;37:2133–5.
[25] Pu M, Feng Q, Wang M, et al. Ultrathin broadband nearly perfect absorber with symmetrical coherent illumination. Opt Express 2012;20:2246–54.
[26] Costa F, Monorchio A, Manara G. Analysis and design of ultra thin electromagnetic absorbers comprising resistively loaded high impedance surfaces. IEEE Trans Antennas Propag 2010;58:1551–8.
[27] Costa F, Monorchio A, Manara G. Efficient analysis of frequency-selective surfaces by a simple equivalent-circuit model. IEEE Antennas Propag Mag 2012;54:35–48.
[28] Langley RJ, Parker EA. Double-square frequency-selective surfaces and their equivalent circuit. Electron Lett 1983;19:675–7.
[29] Langley RJ, Parker EA. Equivalent circuit model for arrays of square loops. Electron Lett 1982;18:294–6.
[30] Pu M, Ma X, Guo Y, et al. Theory of microscopic meta-surface waves based on catenary optical fields and dispersion. Opt Express 2018;26:19555–62.
[31] Hibbins AP, Yakovlev AB, Butler CAM, et al. Circuit modeling of the transmissivity of stacked two-dimensional metallic meshes. Opt Express 2010;18:13309.

[32] Pu M, Guo Y, Li X, et al. Revisitation of extraordinary Young's interference: from catenary optical fields to spin–orbit interaction in metasurfaces. ACS Photonics 2018;5:3198–204.
[33] Zhang M, Pu M, Zhang F, et al. Plasmonic metasurfaces for switchable spin-orbit interactions based on phase change materials. Adv Sci 2018. DOI: 10.1002/advs.201800835.
[34] Luo X. Principles of electromagnetic waves in metasurfaces. Sci China Phys Mech Astron 2015;58:594201.

Supplementary Material The online version of this article offers supplementary material (https://doi.org/10.1515/nanoph-2018-0110).